This article has been accepted for publication in a future issue of this journal, but has not been fully edited. Content may change prior to final publication. Citation information: DOI 10.1109/TIE.2020.2996140, IEEE Transactions on Industrial Electronics

Flux-Modulated Relieving-DC-Saturation Hybrid Reluctance Machine with Synthetic Slot-PM Excitation for Electric Vehicle In-Wheel Propulsion

Xing Zhao, Shuangxia Niu *IEEE Senior Member,* Xiaodong Zhang, Weinong Fu

***Abstract*—The reluctance machine with DC field coils in stator, is an emerging brushless candidate for in-wheel direct drive for its wide speed range and robust mechanical structure, while it suffers from relatively low torque density and efficiency, due to the poor excitation ability of DC field coils and worse extra DC saturation effect in stator core. To address this issue, a new hybrid reluctance machine is proposed in this paper, in which an integrated dual-layer PM source is introduced into stator slots, aiming to relieve DC saturation and meanwhile evoke flux modulation effect. In this way, the stator core utilization factor can be boosted due to DC saturation elimination by inner-layer slot PMs. On the other side, extra PM torque is generated by flux modulation effect of outer-layer slot PMs. Hence, with synthetic assistance from dual-layer slot PMs, the torque density is improved distinctly especially under relatively high current density. Besides, slot PMs share a parallel magnetic circuit with DC field coils, which enables a bidirectional DC magnetization control for speed range extension. In this paper, the proposed new topology is fully evaluated by both finite element analysis and prototype experiments.**

***Index Terms*—DC saturation, flux modulation, magnetic field regulation, synthetic slot PMs, torque density.**

I. Introduction

For modern electric vehicles (EV), using in-wheel machines to provide propulsion power has been regarded as one important trend, since it owns significant vehicle-level advantages such as improved dynamics index, enlarged inner space by elimination of mechanical transmission device, and higher efficiency of the whole drive system [1-5]. There are two typical configurations of in-wheel machines. One candidate is combing a high-speed machine and reduction gearbox, but it suffers from mechanical loss. The other is using a low-speed direct-drive machine.

The traditional permanent magnet (PM) machines, including interior PM machine (IPM) and surface-mounted PM machine (SPM), have been well explored for EV applications. IPM owns high torque density and wide speed range, but it has large torque ripple ratio due to non-sinusoidal magnetic field [6-7]. SPM can obtain good torque density and low torque ripple, while its flux weakening ability is poor due to zero magnetic saliency [8-9]. In the recent years, with a limited supply and price fluctuation of rare-earth PMs, the cost of traditional PM machines shows a distinct growth. Thus, developing high-performance reluctance machines has attracted more attention in literature [10-12].

Switched reluctance machine (SRM) is a potential non-PM solution [13]. SRM owns a robust and fault-tolerant structure, while the torque density of SRM is poor than that of traditional PM machines, since the cores of SRM can only operate in the first quadrant of BH curve. Some design techniques featured by slot PMs have been proposed to extend core BH working range in SRM and thus boost torque density [14-16]. Meanwhile, the torque ripple in SRM is severe due to its half-cycle-conducting operation principle, which is the most critical issue of SRM that limits its practical application [17].

Doubly salient machine with DC field coils in stator, namely DC-DSM, is an emerging non-PM solution in the recent years. At the early stage, DC-DSM uses distributed DC field coils and its feasible slot pole combination is similar with those for SRM. With DC field coils, alternating excitation flux is established in DC-DSM [18], which enables it to operate in a whole electrical period. However, its torque ripple ratio is still unacceptable due to rich flux harmonics [19]. To address this issue, variable flux reluctance machine (VFRM) is proposed [20], which employs concentrated DC field coils uniformly wounded on stator teeth. With this change of DC coil layout, the excitation field becomes symmetrical along the air gap circumference and thus more slot pole combinations are allowed in VFRM than that in DC-DSM. Especially, some new slot pole combinations equipped with odd rotor pole pairs are developed, in which all the even-order flux harmonics are cancelled by electromagnetic complementation. Therefore, compared to DS-DSM and SRM, VFRM can obtain smoother torque when driven by sinusoidal current [21].

However, the torque density of VFRM is still not comparable to that of traditional PM machines. On one hand, the excitation ability of DC field coils is poor than that of rare-earth PMs, as it is difficult to generate high magnetomotive force within fixed slot space and thermal limit. On the other hand, DC field coils generates DC magnetization component in stator teeth and yoke, which cannot be utilized for electromagnetic energy conversion. And worse, it increases hysteresis loss and makes the stator core easily saturated [22]. In [23], it is proved, combing consequent-pole slot PMs with DC field coils can improve excitation ability and torque density, benefiting from the magnetic gearing effect. The issue of this solution is not considering stator DC saturation. In [24-26], constructing an opposite PM magnetic bias has been proved as an effective technology to relieve DC saturation and boost torque density under high current density. However, little PM torque can be generated by this PM magnetic bias.

This paper proposes a synthetic method to improve excitation ability and relieve DC saturation, simultaneously, and hence to boost torque density of reluctance machines with DC field coils. Especially, a new topology is proposed, namely flux-modulated relieving-DC-saturation hybrid reluctance machine, featured by dual-layer synthetic slot PM excitation. This paper is organized as follows. In Section II, the machine configuration and design principle are introduced in detail. In Section III, the slot pole combinations and the determination of dual-layer slot PM usage are illustrated. In Section IV, the electromagnetic performance

Manuscript received November 23, 2019; revised January 05, 2020; March 09, 2020; Accepted May 06, 2020. This work was supported by Project No. 152509/16E under the Research Grant Council, Hong Kong

Xing Zhao, Shuangxia Niu and Weinong Fu are with the Department of Electrical Engineering, The Hong Kong Polytechnic University. Xiaodong Zhang is with Shenzhen In Drive Amperex Co. Ltd, China (Corresponding author: Xiaodong Zhang, e-mail: xiaodong@eee.hku.hk).

This article has been accepted for publication in a future issue of this journal, but has not been fully edited. Content may change prior to final publication. Citation information: DOI 10.1109/TIE.2020.2996140, IEEE Transactions on Industrial Electronics

of this new topology is evaluated by finite element analysis. In Section V, a prototype is built, and experiments are conducted. Finally, some conclusions are drawn in Section VI.

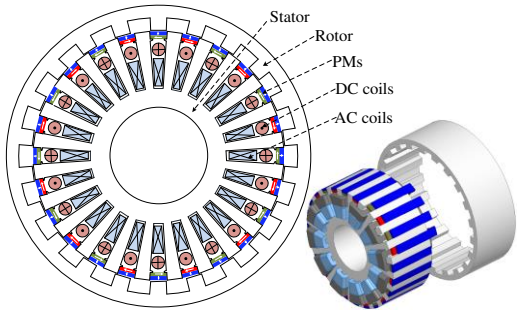

Fig. 1. Structure of the proposed FM-RDCS-HRM.

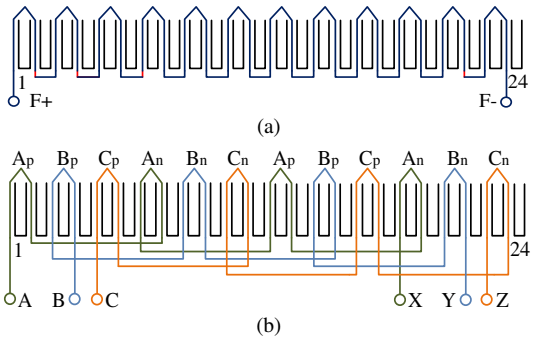

Fig. 2. Winding connections. (a) DC field winding. (b) AC armature winding.

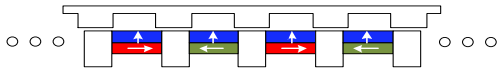

Fig. 3. Magnetization mode for dual-layer slot PMs.

II. The Proposed Machine

A. Machine Configuration

Fig.1 presents the structure of the proposed topology that can be referred as flux-modulated relieving-DC-saturation hybrid reluctance machine (FM-RDCS-HRM). The proposed machine adopts an out-rotor mechanical structure to obtain larger air gap radius and thus higher torque density for in-wheel direct drive. It consists of a 24-slot stator and a 22-pole-pair rotor. All the excitation components are placed in stator slots, while the rotor consists of iron core only. Two sets of concentrated windings are wound, namely DC field winding and AC armature winding, respectively. Their detailed connections are presented in Fig. 2. The DC and AC hybrid excitation contributes to the reluctance torque generation in the proposed FM-RDCS-HRM. However, compared to PMs, using DC field winding is difficult to achieve high magnetomotive force within a fixed slot space and thermal limit. And worse, it brings DC saturation in stator core, thus the excited torque by DC field winding is relatively weak. To solve this problem, a dual-layer slot PM excitation is introduced. The magnetization directions of dual-layer slot PMs are illustrated in Fig. 3. The inner-layer slot PMs are tangentially magnetized in alternate directions, aiming to create a constant PM flux bias to relieve DC saturation in stator core. The outer-layer slot PMs are all magnetized in the same radially outward direction, which can cooperate with adjacent stator teeth and function as a multi-pole PM source to produce flux modulation effect.

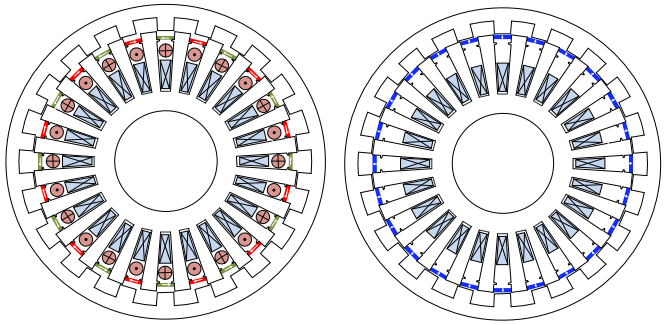

Fig. 4. Structure separation for slot PMs based on electromagnetic interaction. (a) For inner-layer slot PMs. (b) For outer-layer slot PMs.

The advantages of the proposed machine are listed as
(1) The rotor consists of iron core only, which provides a better mechanical robustness compared to rotor-excited counterparts.
(2) The single-layer concentrated winding design brings benefit of eliminated layer isolation, higher slot space factor, shortened winding ends and reduced copper loss.
(3) The inner-layer slot PMs eliminate the DC saturation effect in stator and thus the core utilization factor is boosted. Besides, the outer-layer slot PMs produce extra PM torque based on flux modulation effect. Therefore, the torque density of the proposed topology can be improved significantly, compared to that in the traditional non-PM reluctance machines.
(4) The bidirectional controllability of DC field terminal gives an extra magnetization control variable during flux weakening, which can cooperate with vector control to realize optimal flux weakening operation and extended torque speed range.
(5) With PM arranged in stator slots, the PM magnetic circuit is in parallel with the armature magnetic circuit. Therefore, there is little demagnetization risk for slot PMs.

B. Structure Separation for Dual-Layer Slot PMs

To explain the operation principle of the proposed topology, the dual-layer slot PMs are separated in two different structures as illustrated in Fig. 4. One is a stator-DC-excited reluctance machine equipped with relieving-DC-saturation effect provided by the inner-layer slot PMs, as described in Fig. 4(a). The other is a slot-PM-excited reluctance machine as shown in Fig. 4(b), which operates based on the flux modulation effect excited by the outer-layer slot PMs. For a simplified analysis, the coupling effect between the dual-layer slot PMs is ignored at unsaturated status, and hence the influence of each-layer slot PMs on torque generation can be individually analyzed as follows.

C. Relieving-DC-Saturation Effect of Inner-layer Slot PMs

Fig. 5 presents the schematic flux distribution excited by DC field coils and inner-layer slot PMs with rotor position changing. As illustrated in Fig. 5(a), when the rotor salient pole is aligned with the wounded stator tooth, the loop reluctance for DC field excitation is minimized. Therefore, the flux linkage excited by DC field excitation reaches the maximum value. After the rotor rotates 1/2 pole-pitch and the wounded stator tooth instead faces the rotor slot as shown in Fig. 5(b). The loop reluctance for DC field excitation is maximized and thus the excited flux linkage reaches the minimum value. Therefore, as presented in Fig. 6(a), with the rotor rotation, alternating flux linkage and back EMF can be established for reluctance torque generation.

This article has been accepted for publication in a future issue of this journal, but has not been fully edited. Content may change prior to final publication. Citation information: DOI 10.1109/TIE.2020.2996140, IEEE Transactions on Industrial Electronics

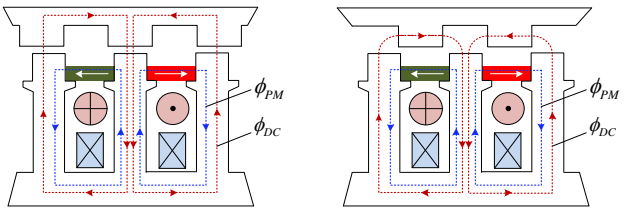

Fig. 5. Schematic flux distribution excited by DC coils and inner-layer slot PMs. (a) Position a, maximum flux linkage. (a) Position b, minimum flux linkage.

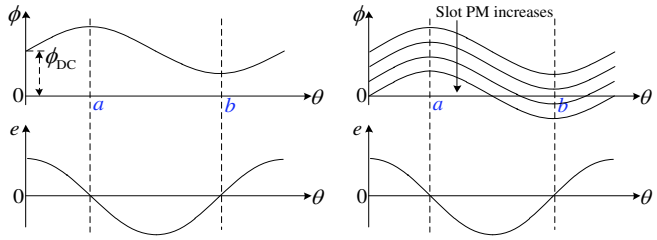

Fig. 6. Schematic flux linkage and back EMF. (a) Without inner-layer slot PMs. (b) With the increase of inner-layer slot PMs

By using Fourier Series, the coil flux linkage excited by DC field coils can be further expanded as

$$\varphi_{coil} = \varphi_{dc} + \sum \varphi_n \sin(n\omega t + \theta_n), n = 1, 2, 3... \quad (1)$$

where φ_{dc} is the DC flux bias, φ_n is the magnitude of the nth flux harmonics, ω is the electrical angle velocity, t is the time, θ_n is the initial phase. Based on a magnetomotive force (MMF) and permeance model, φ_{dc} can be expressed as

$$\varphi_{dc} = N_{dc} i_{dc} \cdot \Lambda_{\text{ave}} \cdot \theta_{st} d_{so} l \quad (2)$$

where N_{dc} is the DC coil turns, i_{dc} is the DC current magnitude, Λ_{ave} is average permeance of DC flux loop, θ_{st} is arc of stator teeth, d_{so} is the outer diameter of the stator, and l is stack length. This DC flux bias cannot produce energy conversion, and worse, it intensifies the saturation of stator core. Hence, the inner-layer slot PMs are adopted to excite relieving-DC-saturation (RDCS) effect. As shown in Fig. 5, regardless of the rotor position, the slot PMs always link the stator core for the minimum reluctance principle. This constant PM flux can be utilized to cancel the DC flux bias. As illustrated in Fig. 6(b), with a certain inner-layer slot PMs, the DC flux bias can be decreased to zero, at which the optimal RDCS operation is achieved. The usage of slot PMs for optimal RDCS operation can be determined by

$$H_c h_{pms} \cdot \Lambda_s \cdot \theta_{st} d_{so} l = \varphi_{dc} \quad (3)$$

where H_c is the coercivity of the slot PMs, h_{pms} is height of slot PMs, Λ_s is average permeance of slot PM flux loop. With this RDCS operation, the maximum flux density in stator core can be reduced, which enhances core utilization factor.

By differentiating the magnetic co-energy with respect to the rotor mechanical position under a constant armature current, the torque equation excited by AC and DC hybrid excitation at the non-saturation status can be derived as

$$T_e = \frac{\delta w_c}{\delta \theta_r} \Big|_{i=\text{constant}} \quad (4)$$

where w_c is the magnetic co-energy and can be written as

$$w_c = \frac{1}{2} L_f i_{dc}^2 + \frac{1}{2} L_p i_{ac}^2 + L_{pf} i_{ac} i_{dc} \quad (5)$$

where L_p, L_f, L_{pf} refer to the self-inductance of AC coil and DC coil as well as their mutual-inductance, respectively. i_{ac}, i_{dc} are the AC current and DC current, respectively. Substituting (2) into (1), the torque equation can be deduced as

$$T_e = \frac{1}{2} i_{dc}^2 \frac{dL_f}{d\theta_r} + \frac{1}{2} i_{ac}^2 \frac{dL_p}{d\theta_r} + i_{ac} i_{dc} \frac{dL_{pf}}{d\theta_r} \quad (6)$$

The first term in the torque equation refers to the cogging torque excited by the variation of magnetic energy product in DC coils. The second term refers to the reluctance torque excited by the self-inductance variation of AC coils only, which cannot make effective torque contribution in the proposed machine. The third term refers to the effective reluctance torque contributed by the mutual-inductance variation between AC and DC coils.

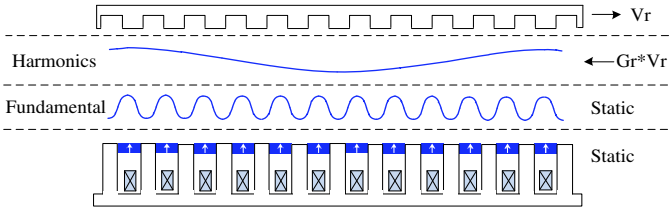

Fig. 7. Illustration of flux modulation effect of outer-layer slot PMs.

D. Flux Modulation Effect of Outer-Layer Slot PMs

Although the inner-layer slot PMs mitigate the DC saturation effect in stator core and boost the reluctance torque generation, the torque density is still not comparable to that in conventional PM machines due to the poor excitation ability of DC field coils. Hence, the outer-layer slot PMs are introduced, aiming to create extra PM torque and further boost the whole torque density.

As shown in Fig. 7, the operation principle of the outer-layer slot PMs is based on the flux modulation effect. Each slot PM and adjacent stator tooth form a pair of magnetic poles. Further, the PM magnetic field is modulated by rotor salient poles and a various air gap harmonics are induced, whose pole pair number $\text{PPN}_{u,v}$ and rotational speed $\omega_{u,v}$ can be predicated by [23]

$$\begin{cases} \text{PPN}_{u,v} = |up_s \pm vp_r| \\ \omega_{u,v} = \dfrac{vp_r}{up_s \pm vp_r} \cdot \omega_r, \quad u = 1, 3, 5..., v = 0, 1, 2, 3.. \end{cases} \quad (7)$$

TABLE I
Dominant harmonics excited by outer-layer slot PMs

	u=1, v=0	u=1, v=1	
$\text{PPN}_{u,v}$	p_s	$p_s + p_r$	$\lvert p_s - p_r \rvert$
$\omega_{u,v}$	0	$\dfrac{p_r}{p_s + p_r}\omega_r$	$\dfrac{p_r}{p_s - p_r}\omega_r$

where p_s is the PPN of outer-layer slot PMs. p_r is the number of rotor salient poles. Among all these air gap harmonics, three components are dominant as presented in Table I. The first item refers to the fundamental PM field without rotor modulation. The rotation speed of fundamental PM harmonic is zero, thus cannot produce effective torque generation. The second and the third items are the dominant PM harmonics generated by rotor modulation. To transmit steady torque with PM harmonics, the

This article has been accepted for publication in a future issue of this journal, but has not been fully edited. Content may change prior to final publication. Citation information: DOI 10.1109/TIE.2020.2996140, IEEE Transactions on Industrial Electronics

relation between the PPN of AC armature winding p_a, the PPN of out-layer slot PMs, and the number of rotor salient poles, should be governed by

$$p_a = |p_s - p_r| \tag{8}$$

The magnetic gearing ratio can be further written as

$$G_r = \frac{p_s}{p_a} \tag{9}$$

The torque produced by outer-layer slot PMs can be derived by differentiating the magnetic co-energy as

$$T_{pm} = \frac{3}{2} \cdot k_w r_g l_a p_r \frac{B_p}{G_r} \cdot NI \tag{10}$$

where k_w is the fundamental winding factor, r_g is the air-gap radius, l_a is the stack length, B_p is the amplitude of harmonic flux density, and NI is the winding ampere turns.

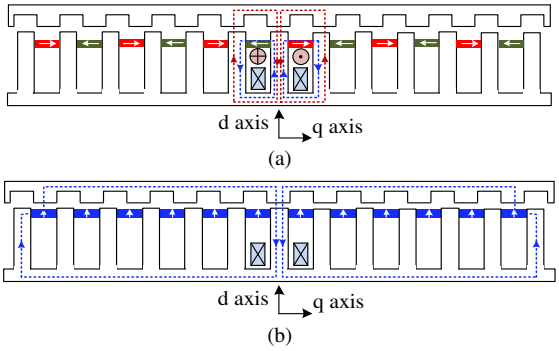

Fig. 8. Illustration of the maximum excitation flux linkage of single AC coil. (a) DC field coils with inner-layer slot PMs. (b) With outer-layer slot PMs only.

E. Integration Effect of Dual-Layer Slot PMs and DC Coils

Fig. 8 illustrates the flux distribution of different excitation sources. It is shown, the DC field coils and outer-layer slot PMs produce the maximum excitation flux linkage at the same rotor position, which means the flux linkage of these two excitation sources have the same phase angle. It should be also mentioned the inner-layer slot PMs have no influence on flux phase angle of DC coils. Further, the electrical frequency of flux linkage in the proposed topology can be determined by

$$f = \frac{n}{60} N_r \tag{11}$$

Where n is the machine speed. N_r is the number of rotor salient poles. Although the pole pair number of outer-layer slot PMs and DC field coils are different, the electrical frequency of flux linkage produced by these two excitation sources are the same, since it's not influenced by the pole pairs of excitation source at stator side. This is different from traditional PM machines in which the PMs are located at the rotor side and its flux electrical frequency is proportional to the PM pole pairs.

In general, the flux linkage of DC field coils and outer-layer slot PMs can be integrated without any phase shift or internal loss, due to the same electrical frequency and same phase angle. This flux linkage integration means that the torque components generated by these two excitation sources can overlap together. Compared to the non-PM counterpart, the outer-layer slot PMs bring extra PM torque, thus leading to the torque density boost. Moreover, the synthetic flux linkage can be flexibly adjusted by regulating DC current. This DC magnetization control can be coordinated with the conventional vector control to achieve the optimal torque speed range in the proposed machine.

F. Drive System and Control Strategy

Fig. 9 illustrates the drive system and control strategy for the proposed FM-RDCS-HRM. The drive system mainly consists of a DC power source, a three-phase inverter for AC armature terminal and an H-bridge converter for DC field terminal. The control strategy has three blocks, namely Id=0 maximum torque per ampere (MTPA) vector control block, Id<0 flux weakening vector control as well as DC magnetization control. When the machine operates under the base speed, full DC magnetization control should be employed and combined with Id=0 MTPA vector control to maximize the torque for fast starting. Once the machine runs over base speed, continuous DC demagnetization control can be coordinated with i_d <0 FW vector control, thus to obtain the optimal torque performance in the high-speed region. Specifically, during FW operation, the voltage limit and current limit under dq coordinate system can be expressed as

$$\begin{cases} (u_d + u_0)^2 + u_q^2 \le u_{dc}^2 \\ i_d^2 + i_q^2 \le i_{s\max}^2 \end{cases} \tag{12}$$

where u_0 is the no-load back EMF. u_{dc} is the DC bus voltage. i_{smax} is the inverter current scale. In the proposed machine, u_0 can be continuously decreased by DC demagnetization control, leading to the change of working point during FW operation as illustrated in Fig. 10. It is shown with extra DC demagnetization control, reduced i_d current is required to satisfy the voltage limit during FW operation, and thus larger i_q current can be allowed for torque generation under a fixed inverter current scale.

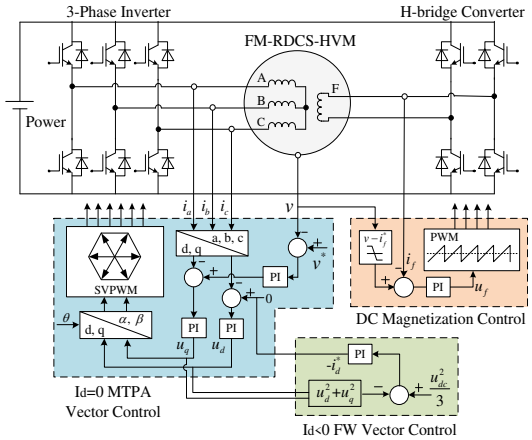

Fig. 9. Drive system and control strategy for the proposed FM-RDCS-HRM.

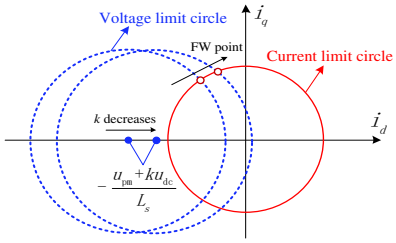

Fig. 10. Variation of current and voltage limits during flux weakening operation by DC demagnetization control. (k refers to the FW coefficient of DC terminal).

This article has been accepted for publication in a future issue of this journal, but has not been fully edited. Content may change prior to final publication. Citation information: DOI 10.1109/TIE.2020.2996140, IEEE Transactions on Industrial Electronics

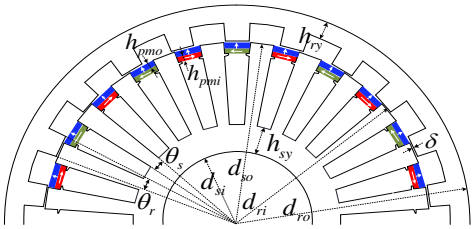

Fig. 11. General dimension parameters.

TABLE II
Design Parameters for the Proposed FM-RDCS-HRM

Symbol	Parameter	Unit	Value
d_{ro}	Outer diameter of rotor	mm	150
d_{ri}	Inner diameter of rotor	mm	130
d_{so}	Outer diameter of stator	mm	129
d_{si}	Inner diameter of stator	mm	60
h_{ry}	Height of rotor yoke	mm	5
h_{sy}	Height of stator yoke	mm	10
h_{pmo}	Height of outer-layer slot PMs	mm	Variable
h_{pmi}	Height of inner-layer slot PMs	mm	Variable
δ	Air gap length	mm	0.5
l	Stack length	mm	80
θ_s	Arc of stator teeth	°	Variable
θ_r	Arc of rotor salient pole	°	Variable
	Turns of each DC coil	-	50
	Turns of each AC coil	-	50
	Wire size (AWG)	-	30
	Slot factor	-	0.7

III. Design Considerations

A. Slot Pole Combination

The feasible slot pole combinations in the proposed machine can be expressed as [20]

$$\begin{cases} N_s = 2mj,\ j = 1,2,3\ldots \\ N_r = N_s \pm 2k,\ k = 1,2,3\ldots \end{cases} \tag{13}$$

where m is the phase number. N_s is the number of stator slots. The designs having odd rotor pole pairs are not recommended due to the influence of unbalanced magnetic pull. Further, based on the flux modulation effect, N_r should be designed in close to N_s to achieve relatively high magnetic gearing ratio and torque density. Using a 24-slot stator, four potential slot pole designs, 24/20, 24/22, 24/26 and 24/28 are compared in this paper.

Finite element (FE) method is adopted for machine modeling and performance evaluation. The general dimension parameters are labeled in Fig. 11, with their design values listed in Table II. For a fair comparison, the height of inner-layer and outer-layer slot PMs are both keep at 2mm for all the slot pole combinations. The arc of stator teeth and rotor salient pole are both optimized for each case. Fig. 12 shows the calculated armature inductance of four designs. It can be seen, for 24/20 and 24/28 cases, their armature inductances vary with the electrical angle, while those of 24/22 and 24/26 designs maintain constant almost. Table III presents calculated torque performance. It is shown, the 24/20 design can obtain the maximum average torque, but its cogging torque and torque ripple are also much larger than other designs. When the minimum torque ripple ratio and cogging torque ratio are considered as the selection criteria, the 24/22 case is the best design for further study. The difference of torque performance is due to the inductance difference, which determines reluctance torque distribution and influences torque ripple greatly [20].

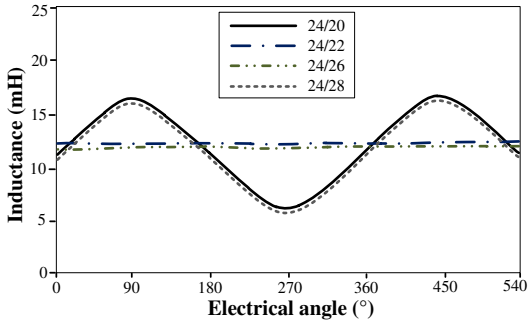

Fig. 12. Armature inductances with four slot pole combinations

TABLE III
Torque Performance with Four Slot Pole Combinations

N_s	24	24	24	24
N_r	20	22	26	28
θ_s (°)	7.2	6.8	6.9	7.1
θ_r (°)	8.2	7.6	6.4	5.8
Current density (A/mm^2)	6	6	6	6
Cogging torque (Nm)	1.8	0.7	0.8	1.6
Torque ripple (Nm)	2.6	1.1	1.2	2.2
Average torque (Nm)	13.5	12.4	12.1	11.2

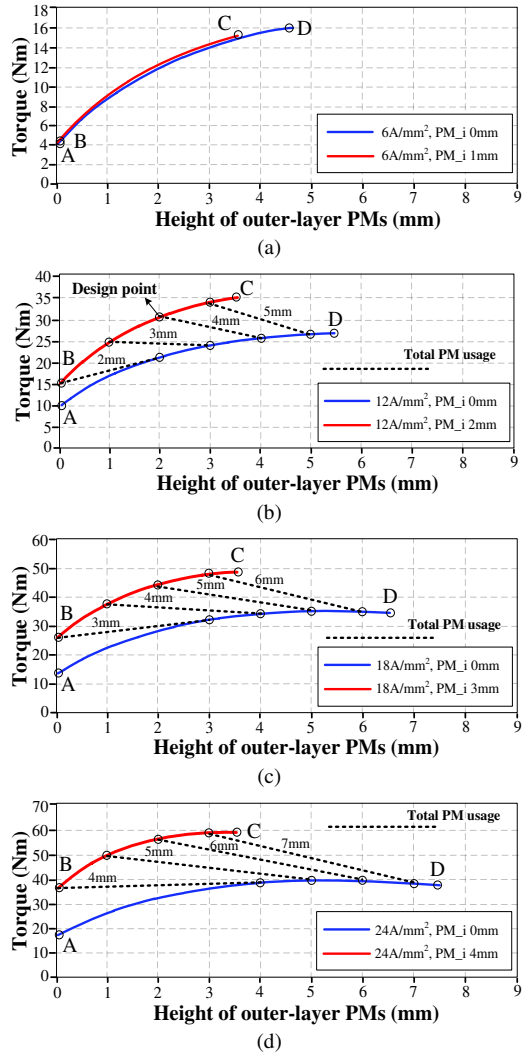

Fig. 13. Examination of RDCS operation on torque ability considering different current density. (a) 6A/mm^2. (b) 12 A/mm^2. (c) 18 A/mm^2. (d) 24 A/mm^2. Four typical design cases of A, B, C, D are selected and denoted in figure, with their corresponding schematic illustrations presented as bellow

This article has been accepted for publication in a future issue of this journal, but has not been fully edited. Content may change prior to final publication. Citation information: DOI 10.1109/TIE.2020.2996140, IEEE Transactions on Industrial Electronics

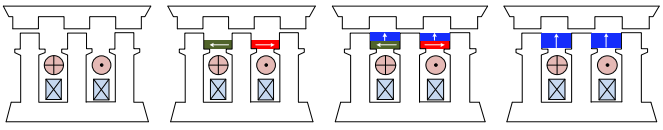

Case A: the original non-PM topology.
Case B: the topology with only inner-layer slot PMs.
Case C: the proposed topology dual-layer slot PMs
Case D: the topology with only outer-layer slot PMs.
The Case C and Case D share the same total PM usage.

B. Determination of Dual-Layer PM Usages

The determination principles of dual-layer PM usages can be illustrated as follows. (1) Under a given current excitation, the optimal usage of inner-layer slot PMs can be determined as long as the coil flux linkage has zero DC bias. Overuse of inner-layer slot PMs not only increases cost, but also brings negative DC bias and thus DC saturation effect. (2) Then, the optimal usage of outer-layer slot PMs can be determined to provide maximum PM torque with minimum PM usage, considering that overuse of outer-layer slot PMs cannot contribute to PM torque increase due to the global saturation effect.

Moreover, to verify the effectiveness of RDCS operation by inner-layer slot PMs, two solutions are comparatively studied. One is the proposed topology with dual-layer slot PMs, and the other is the existing one in which only outer-layer slot PMs are adopted [27]. Fig. 13 presentss the influence of PM usage on the torque ability of two solutions with different current density. Four typical cases of A, B, C, D are denoted in Fig. 13.

As presented in Fig. 13(a), when 6A/mm^2 current excitation is applied, the inner-layer slot PMs contribute few torque. This is because DC saturation effect is not so significant under small this current excitation. With the increase of current excitation, the torque boost by inner-layer slot PMs due to DC saturation elimination becomes more and more distinct, as can be found by comparing Case A and Case B in Fig. 13 (b) and (c), and (d), respectively. It is shown, with large current excitation applied, the torque ability of the proposed topology with dual-layer slot PMs, is obviously higher than that of the existing topology with only outer-layer slot PMs even when they are designed with the same total PM usage. More specially, by comparing Case C and Case D, 27.2% higher torque density of the proposed topology can be observed under 12A/mm^2 current excitation. This data increases to 45.1% under 18A/mm^2 and 50.3% under 24A/mm^2, respectively. The reason for this is, with the increase of current excitation, the DC flux bias in stator core becomes larger as well, and its limit on torque ability cannot be neglected due to extra DC saturation. Meanwhile, the PM torque boost of outer-layer slot PMs is also restricted due to global saturation.

As reported in literature [28], the rated current density of the commercial automotive IPM can be designed at 24A/mm^2 using an oil-cooling method. For the proposed machine, its rated point is designed at 12A/mm^2 using a strong fan-cooling method for a short-time period laboratory test. It can be seen in Fig. 13(b), at current density of 12A/mm^2, when the total PM usage is 2mm and 3mm, the torque excited by dual-layer slot PMs is lower than that excited by outer-layer slot PMs only. This is because, the stator core is not saturated at these points and thus the RDCS operation of inner-layer slot PMs makes little contribution to torque boost. When the total PM usage is larger than 4mm, the magnetic load increases and stator core is in close to saturation. Therefore, the RDCS operation becomes effective now and thus the torque of dual-layer slot PMs becomes more advantageous, while the torque excited by outer-layer slot PMs only is limited by global saturation. Specifically, when using inner PMs 2mm plus outer PMs 2mm, about 20% higher torque can be observed compared to using outer PMs 4mm. And when using inner PMs 2mm plus outer PMs 3mm, about 25% higher torque is achieved compared to using outer PMs 5mm. Therefore, it's feasible to determine the total PM usage to be either 4mm, 5mm, or larger. Our considerations to select the design point is based on the PM cost limit and our torque test ability. On one hand, the 2mm plus 2mm design can already demonstrate the torque density boost with our proposed dual-layer PM topology, thus increasing PM usage is not necessary considering the cost limit. On the other hand, our torque test ability is limited by laboratory instruments, thus increasing PM usage may exceed the test range.

IV. Electromagnetic Performance Analysis

A. Magnetic Field Distribution

Fig. 14 presents the no-load magnetic field distribution of the proposed machine at different excitation status. When only DC current of 12A is applied as shown in Fig. 14(a), the effective flux starts from the wound stator tooth, then enters rotor salient pole, and finally comes back through two adjacent stator teeth. This flux linkage contributes to the reluctance torque generation. However, the flux density of stator core is obviously higher that of rotor core due to the existence of DC flux bias, which makes the stator core easier to be saturated. By introducing inner-layer slot PMs of 2mm, as presented in Fig. 14(b), the flux density of stator core can be reduced significantly, while that of rotor core keeps unchanged almost, which proves inner-layer slot PMs can relieve DC saturation in the stator core. Fig. 14(c) and Fig. 14(d) present the situations with outer-layer slot PMs of 2mm applied. The outer-layer slot PMs elevate the flux density of both stator core and rotor core, and saturation already occurs at stator teeth if no inner-layer slot PMs are applied as presented in Fig. 14(c). Therefore, by coordinating the inner-layer and outer-layer PMs, the flux density distribution of the stator core and rotor core can be more uniform as can be found in Fig. 14(d).

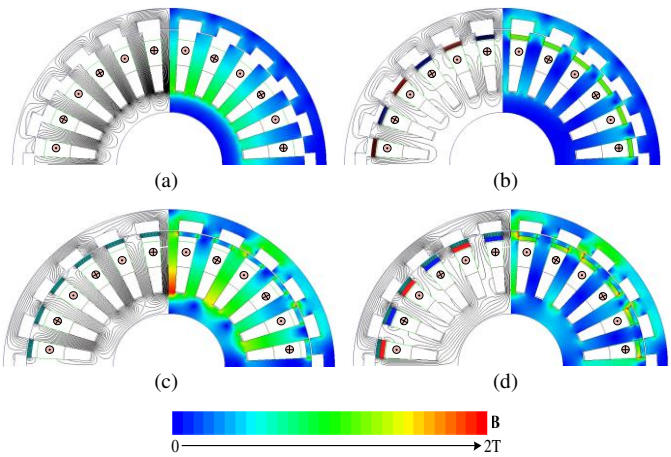

Fig. 14. Magnetic field distribution. (a) idc 12A/mm^2 only. (b) idc 12A/mm^2 and inner-layer PMs 2mm. (c) idc 12A/mm^2 and outer-layer PMs 2mm. (d) idc 12A/mm^2, inner-layer PMs 2mm and outer-layer PMs 2mm.

This article has been accepted for publication in a future issue of this journal, but has not been fully edited. Content may change prior to final publication. Citation information: DOI 10.1109/TIE.2020.2996140, IEEE Transactions on Industrial Electronics

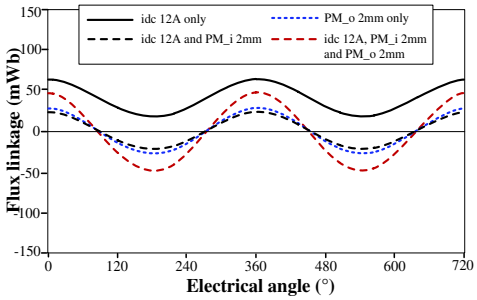

Fig. 15. Coil flux linkage at different excitation status.

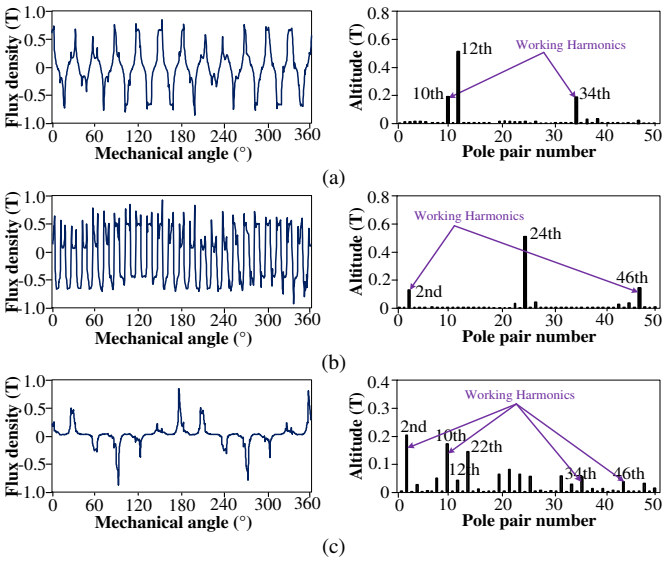

Fig. 16. Flux density in air gap and its harmonics distribution. (a) Only idc 12A. (b) Only outer-layer slot PMs. (c) Only AC armature current 12A.

Fig. 15 shows the calculated no-load flux linkage of each coil at different excitation status. It is shown, with the introduction of inner-layer slot PMs, the DC bias of coil flux linkage can be eliminated. Meanwhile, the flux component of outer-layer slot PMs is entirely in phase with that of DC current, and thus they can overlap effectively without any inner cancellation.

Fig. 16 presents the calculated air gap flux density excited by different sources, with their harmonic spectrum obtained by fast Fourier Analysis. According to the flux modulation theory, the excitation harmonics with the same rotation speed and pole pair number as that of armature harmonics can work effectively and contributes to steady torque generation. As shown in Fig. 16(a) and Fig. 16(b), the air gap harmonics produced by DC current and out-layer slot PMs are entirely different. Their fundamental harmonics cannot work since they are both stationary. For the armature field, with a single-layer concentrated winding design, plentiful air gap harmonics are excited, which can interact with both DC field and PM field for torque generation.

B. *Inductance Characteristic*

The no-load inductance characteristic is evaluated in Fig. 17. As illustrated in Fig.2(b), according to the phase relation, the adjacent coils of one phase are split into two sub phases, namely sub-phase Ap and An, respectively, taking phase A as example. It is shown that, the general self-inductance of one phase keeps constant almost, while the self-inductance of each sub phase varies periodically, which leads to reluctance torque. Moreover, the mutual inductance between phases can be ignored almost.

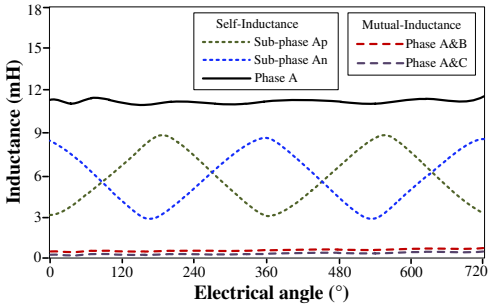

Fig. 17. Self-inductance and mutual-inductance.

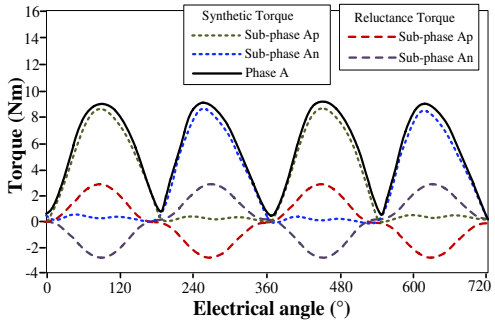

Fig. 18. Reluctance torque components with current density of 12A/mm^2.

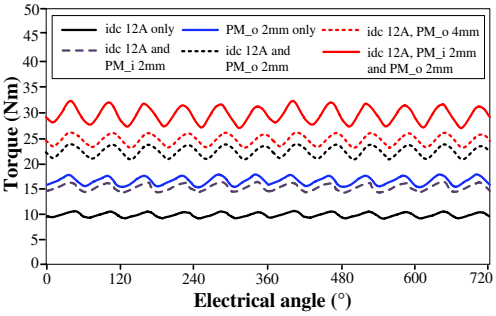

Fig. 19. Steady torque components with current density of 12A/mm^2.

C. *Torque Components*

Fig. 18 presents the calculated torque components without slot PMs, in which “synthetic torque” refers to the sum of three torque components which can be referred in Equ. (6). It can be seen, the torque components of two sub-phases generated by the variation of self-inductance only, are cancelled due to their 180° phase difference. The effective average torque is contributed by the interaction between AC and DC current excitation, and they are complementary between two sub-phases. Therefore, there is no torque dead zone of one phase in the whole electrical period. Fig. 19 presents the steady torque components with dual-layer slot PMs. It can be seen, with the introduction of inner-layer slot PMs of 2mm, the torque is boosted from about 10Nm to 15Nm. Then, with outer-layer slot PMs of 2mm introduced, the torque grows from 15Nm to 30Nm approximately. Besides, it can be found, the torque with outer-layer slot PMs 4mm is 5Nm lower than that with dual-layer slot PMs of both 2mm, which is due to the RDCS effect as discussed previously.

Further, the torque ability of the proposed design is evaluated against industrial Toyota Prius interior PM machine (IPM) [28]. The comparison results are listed in Table IV. It is shown, when two machines share the same outer dimension, stack length, air gap length as well as current density, the proposed topology has 26.7% higher torque per volume than IPM, while its torque per PM is relatively lower. Besides, in Table IV, the reduced space

of winding ends is not considered with a concentrated design in the proposed topology, which means, within a fixed mechanical space, the torque density of proposed topology can be further improved compared to IPM with distributed winding.

TABLE IV
Comparison of Torque Ability against Industrial IPMs

	FT-RDCS-HRM	IPM [28]
Outer dimension (mm)	268	
Stack length (mm)	50	
Air gap length (mm)	0.75	
PM volume (mm^3)	146400	82960
Current density (A/mm^2)	12	
Torque per volume (kNm/m^3)	31.3	24.7
Torque per PM (Nm/L)	669	732

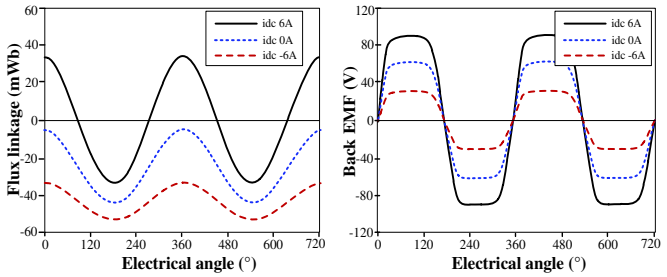

(a) (b)

Fig. 20. Magnetization ability of DC terminal. (a) Flux linkage. (b) Back EMF.

(a) (b)

Fig. 21. PM flux density distribution at full load. (a) idc 12A. (b) idc -12A.

D. DC Magnetization Control

The magnetization control ability of DC terminal is evaluated. As shown in Fig. 20(a), with bidirectional DC current applied, the DC bias of flux linkage can be flexibly adjusted. Especially, with the negative DC current of 6A applied, the DC saturation effect becomes severe, and thus the effective amplitude of flux linkage is reduced significantly. Further, as shown in Fig. 20(b), the back EMF can be weakened by 70% at rated condition.

For a safe operation, the PM demagnetization risk during flux weakening should be examined. In general, the working point of PMs is determined by current magnetomotive force (MMF) and environment temperature at the same time. To examine PM demagnetization behavior in the proposed design, the total loss at the full load condition, including copper loss, core loss and PM eddy current loss, are calculated and then involved into the iteration between electromagnetic field and temperature field. In this way, the PM temperature and corresponding B-H feature can be determined for demagnetization evaluation. For NdFeB magnets, the knee point of irreversible demagnetization is about 0.33T at 125°. Fig. 21 presents the flux density distribution of dual-layer PMs with maximum and minimum DC current at full load. It is shown, the influence of DC current on PM working point is not distinct. Besides, the minimum PM flux density of PMs is about 0.45T, thus no demagnetization exists.

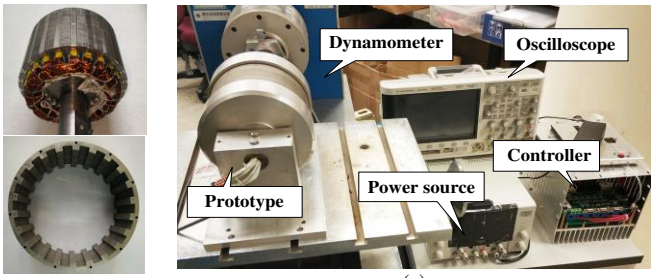

(a) (c)

Fig. 22. (a) Prototype details including stator and rotor. (b) Test platform.

TABLE V
Specifications and Materials of the Prototype

Specifications		Materials		
Rated speed	1000 rpm	PM	Type	NdFeB35
Rated current density	12 A/mm^2		Remanence	1.2 T
Rated power	3140 W		Coercive force	915 kA/m
Peak power	5500 W	Steel	Type	MG19_24
Phase inductance	12 mH		Saturated point	1.8 T
Phase resistance	0.64 Ω		Mass density	7650 kg/m^3

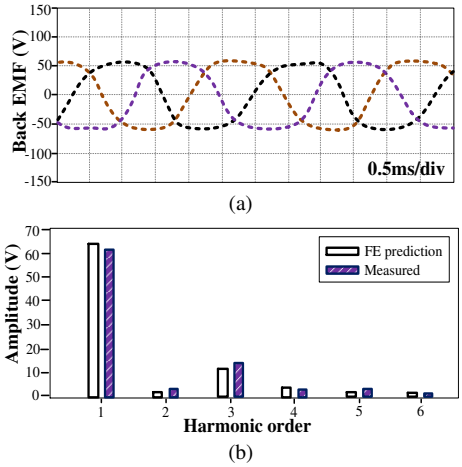

(a) (b)

Fig. 23. (a) Back EMF without DC current. (b) Harmonics distribution.

V. Experimental Verification

A prototype is fabricated and tested. Relevant dimensions are in line with those listed in Table II, and the inner-layer PM and outer-layer PM are both set 2mm. The major specifications and materials are given in Table V. Fig. 22(a) shows the details of prototype. In the stator assembly, dual-layer PMs are mounted on slot openings. Each PM is joined by two segments to reduce PM eddy current loss. With a single-layer concentrated winding, the wiring process is simple, and the winding ends are shortened. In the rotor assembly, the rotor core is connected into two end discs by screw to provide a mechanical support. A test platform is built as shown in Fig. 22(b), which consists of the prototype, dynamometer, drive controller, power source and oscilloscope.

Firstly, the back EMF at 1000rpm without DC current and its harmonic distribution are presented in Fig. 23. It is shown, the measured result basically agrees with FE predication, although its amplitude is a little smaller, due to the influence of different air gap harmonic distribution that may be caused by the uneven PM magnetization. Then, the back EMF values against different DC current are shown in Fig. 24. With bidirectional DC current, the back EMF can be weakened and strengthened as predicated, thus proving the DC magnetization control ability.

This article has been accepted for publication in a future issue of this journal, but has not been fully edited. Content may change prior to final publication. Citation information: DOI 10.1109/TIE.2020.2996140, IEEE Transactions on Industrial Electronics

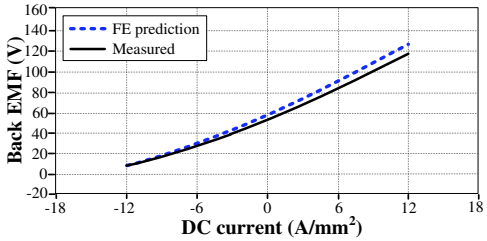

Fig. 24. Back EMF against different DC current.

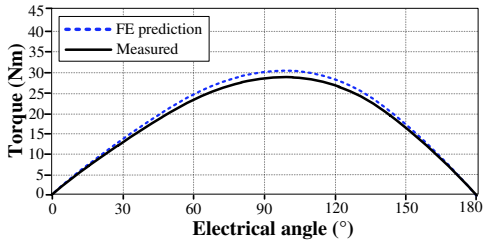

Fig. 25. Torque angle curve with DC current of 12A/mm^2.

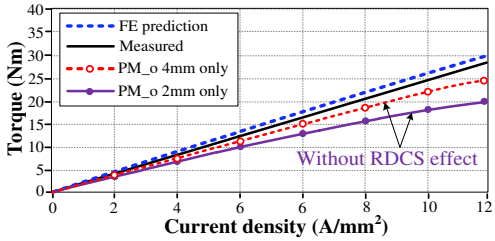

Fig. 26. Torque capacity under different current density

Then, the torque angle curve with DC current 6A is collected by measuring the static torque at different locked rotor positions. As shown in Fig. 25, the tested result agrees with FE prediction, and the control angle to obtain the maximum torque is near 90°, similar with that for the traditional non-saliency PM machines. Fig. 26 presents the tested torque ability under different current density. It can be seen, with the synchronous increasing of both AC and DC current density, the torque saturation trend is not distinct when the current density reaches 12A/mm^2. This is due to the RDCS effect provided by inner-layer slot PMs. Therefore, the proposed machine has good potential for overload operation if the cooling condition is satisfied.

Fig. 27 presents the torque ability in the whole speed region. The DC bus voltage is set 400V and the based speed is 1000rpm. When the machine is operating under based speed, id=0 should be applied to maximum the torque ability during starting. Once the machine operates over based speed, the traditional vector flux weakening should be applied by increasing id current and decreasing iq current to meet the voltage limit and current limit. In the proposed topology, by changing DC current and repeat the above control strategy, relevant torque speed characteristics can be collected as a function of DC current values. It is shown, with the decreasing of DC current, the torque speed region can be extended effectively, which is due to the extra magnetization control ability of DC terminal in flux weakening.

Finally, the rated efficiency of this new topology is examined and compared with the existing topologies. Table VI shows the calculated efficiency of three designs with same rated condition. It is shown, by using dual-layer slot PMs, the proposed design exhibits efficiency improvement as well, which is in line with its torque boost. Therefore, the proposed topology has potential for in-wheel direct-drive applications.

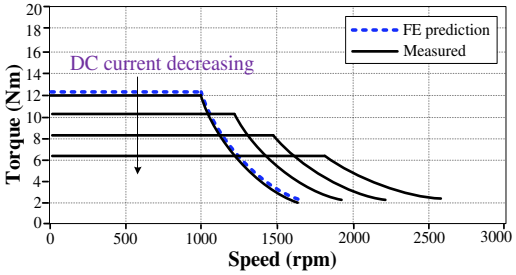

Fig. 27. Torque speed curves, DC current from 6 to -3A/mm^2, step 3A/mm^2.

TABLE VI
Comparison of Rated Efficiency with Different Topologies

	No PMs	Outer-layer PMs only	Dual-layer PMs
Rated speed	1000 rpm		
Current density	12 A/mm^2		
Efficiency	62.5%	79.1%	84.2%

VI. Conclusion

Aiming for the in-wheel direct-drive applications, this paper presents a new flux-modulated relieving-DC-saturation hybrid reluctance machine, which integrates the advantages of boosted torque density and bidirectional magnetization control ability. The innovation is introducing an integrated dual-layer slot-PM excitation to evoke both relieving-DC-saturation effect and flux modulation effect, and thus boost stator core utilization factor and PM torque as well. The proposed machine is evaluated by both finite element analysis and prototype experiments.

It is revealed in this paper, when the machine is designed with small current density, the inner-layer slot PMs contribute to few torque since the DC saturation in stator core due to DC current excitation is not significant. In this situation, it is recommended to use the whole outer-layer slot PMs instead of dual-layer PMs. However, when the machine is designed with relatively high current density, the DC saturation in stator core becomes more distinct, which degrades core utilization factor and essentially limits machine torque ability. In this case, using inner-layer slot PMs is recommended. For our prototype, under current density of 12A/mm^2, using dual-layer PMs contributes to 27.2% higher torque than that when using outer-layer PMs only with the same total PM usage. This data increases to 45.1% under 18A/mm^2 and 50.3% under 24A/mm^2, respectively. It needs to be pointed our prototype is designed at 12A/mm^2 due to the limited cooling condition. In future work, by improving the cooling method, the current density can be increased to fully examine torque ability. Besides, using ferrite magnets can be also explored considering the issue of PM utilization ratio and increased cost burden.

References

[1] A. Emadi, Y. J. Lee, and K. Rajashekara, "Power electronics and motor drives in electric, hybrid electric, plug-in hybrid electric vehicles," *IEEE Trans. Ind. Electron.*, vol. 55, no. 6, pp. 2237–2245, Jun. 2008.

[2] Y. Itoh, K. Sakai, and Y. Makino, "In-wheel motor system," New Technol. Netw. (NTN) Corp., Nishi-ku, Osaka, Japan, Tech. Rev. no. 79, pp. 22–28, 2011.

[3] L. De Novellis, A. Sorniotti, and P. Gruber, "Wheel torque distribution criteria for electric vehicles with torque-vectoring differentials," *IEEE Trans. Veh. Technol.*, vol. 63, no. 4, pp. 1593–1602, May 2014.

[4] A. M. Dizqah, A. M. Dizqah, B. Lenzo, and J. De Smet "A fast and parametric torque distribution strategy for four-wheel-drive energy-efficient electric vehicles," *IEEE Trans. Ind. Electron.,* vol. 63, no. 7, pp. 4367–4376, Jul. 2016.

[5] S. U. Chung, S. H. Moon, D. J. Kim and J. M. Kim, "Development of a 20-Pole-24-Slot SPMSM with consequent pole rotor for in-wheel direct drive," *IEEE Trans. Ind. Electron.*, vol. 63, no. 1, pp. 302-309, Jan. 2016.
[6] J. Nerg, M. Rilla, and S. Ruotsalainen, "Direct-driven interior magnet permanent-magnet synchronous motors for a full electric sports car," *IEEE Trans. Ind. Electron.*, vol. 61, no. 8, pp. 4286–4294, Aug. 2014.
[7] P. B. Reddy, A. M. El-Refaie, K. K. Huh, J. K. Tangudu and T. M. Jahns, "Comparison of interior and surface PM machines equipped with fractional-Slot concentrated windings for hybrid traction applications," *IEEE Trans. Energy Convers,* vol. 27, no. 3, pp. 593-602, Sept. 2012.
[8] D. K. Hong, and B. C. Woo, "Design, analysis, and experimental validation of a permanent magnet synchronous motor for articulated robot applications," *IEEE Trans. Magn.*, vol. 54, no. 3, pp. 1-4, March 2018.
[9] A. M. El-Refaie, T. M. Jahns, P. J. McCleer and J. W. McKeever, "Experimental verification of optimal flux weakening in surface PM Machines using concentrated windings," *IEEE Trans. Ind. Appl.*, vol. 42, no. 2, pp. 443-453, 2006.
[10] I. Boldea, L. N. Tutelea, L. Parsa and D. Dorrell, "Automotive electric propulsion systems with reduced or no permanent magnets: an overview," *IEEE Trans. Ind. Electron.*, vol. 61, no. 10, pp. 5696-5711, Oct. 2014.
[11] C. H. T. Lee, K. T. Chau, C. Liu, and D. Wu, "Quantitative comparison and analysis of magnetless machines with reluctance topologies," *IEEE Trans. Magn*, vol. 49, no. 7, pp. 3969-3972, July 2013.
[12] A. Fasolo, L. Alberti and N. Bianchi, "Performance comparison between switching-flux and IPM machines with rare-earth and ferrite PMs," *IEEE Trans. Ind. Appl*, vol. 50, no. 6, pp. 3708-3716, Nov.-Dec. 2014.
[13] X. D. Xue, K. W. E. Cheng, and T. W. Ng, "Multi-objective optimization design of in-wheel switched reluctance motors in electric vehicles," *IEEE Trans. Ind. Electron.*, vol. 57, no. 9, pp. 2980-2987, Sept. 2010.8
[14] P. Andrada, B. Blanqué, E. Martínez, M. Torrent, "A novel type of hybrid reluctance motor drive", *IEEE Trans. Ind. Electron.*, vol. 61, no. 8, pp. 4337-4345, Aug. 2014.
[15] J. Zhu, K. W. E. Cheng and X. Xue, "Design and analysis of a new enhanced torque hybrid switched reluctance motor," *IEEE Trans. Energy Convers*, vol. 33, no. 4, pp. 1965-1977, Dec. 2018.
[16] S. Ullah, S. P. McDonald, R. Martin, M. Benarous and G. J. Atkinson, "A permanent magnet assist, segmented rotor, switched reluctance drive for fault tolerant aerospace applications," *IEEE Trans on Indus. Appl.*, vol. 55, no. 1, pp. 298-305, Jan.-Feb. 2019.
[17] Y. Jin, B. Bilgin, and A. Emadi, "An extended-speed low-ripple torque control of switched reluctance motor drives," *IEEE Trans. Power Electronics*, vol. 30, pp. 1457-1470, 2015
[18] Y. Wang, Z. Zhang, and Y. Yan, "Torque density improvement of doubly salient electromagnetic machine with asymmetric current Control," *IEEE Trans. Ind. Electron.*, vol. 63, no. 12, pp. 7434-7443, Dec. 2016.
[19] Z. Chen, and Y. Yan "A doubly salient starter/generator with two-section twisted-rotor structure for potential future aerospace application," *IEEE Trans. Ind. Electron.*, vol. 59, no. 9, pp. 3588-3595, Sept. 2012.
[20] X. Liu and Z. Q. Zhu, "Stator rotor pole combinations and winding configurations of variable flux reluctance machines," *IEEE Trans. Ind. Appl*, vol. 50, no. 6, pp. 3675-3684, Nov.-Dec. 2014.
[21] X. Liu and Z. Q. Zhu, "Comparative study of novel variable flux reluctance machines with doubly fed doubly salient machines," *IEEE Trans. Magn.*, vol. 49, no. 7, pp. 3838-3841, July 2013.
[22] S. Xue, J. Feng, S. Guo and Z. Q. Zhu *et al*, "Iron loss model under DC bias flux density considering temperature influence," *IEEE Trans. Magn*, vol. 53, no. 11, pp. 1-4, Nov. 2017
[23] X. Zhao and S. Niu, "Design and optimization of a novel slot-PM-assisted variable flux reluctance generator for hybrid electric vehicles," *IEEE Trans. Energy Convers.*, vol. 33, no. 4, pp. 2102-2111, Dec. 2018.
[24] X. Zhao, S. Niu and W. Fu, "A new modular relieving-DC-saturation Vernier reluctance machine excited by zero-Sequence current for electric vehicle," *IEEE Trans. Magn*, vol. 55, no. 7, pp. 1-5, July 2019.
[25] S. Ullah, and G. J. Atkinson, "A permanent magnet assist, segmented rotor, switched reluctance drive for fault tolerant aerospace applications," *IEEE Trans on Ind. Appl.*, vol. 55, no. 1, pp. 298-305, Jan.-Feb. 2019.
[26] X. Zhao, S. Niu, X. Zhang and W. Fu, "Design of a new relieving-DC-saturation hybrid reluctance machine for fault-tolerant in-wheel direct drive," *IEEE Trans. Ind. Electron.*, early access, 2020.
[27] X. Zhao and S. Niu, "Design of a novel parallel-hybrid-excited Vernier reluctance machine with improved utilization of redundant winding harmonics," *IEEE Trans. Ind. Electron.*, vol. 65, no. 11, pp. 9056-9067, Nov. 2018.
[28] M. Olszewski, "Evaluation of the 2010 Toyota Prius hybrid synergy drive system," Oak Ridge Nat. Lab., U.S. Dept. Energy, 2011.

Xing Zhao received the B.Sc. degree in Electrical Engineering from the Department of Automation, Nanjing University of Aeronautics and Astronautics, China, in 2014, and currently he is pursuing Ph.D. degree in Electrical Engineering at the Department of Electrical Engineering at the Hong Kong Polytechnic University, Hong Kong. In 2019, he was a visiting scholar at Center for Advanced Power Systems, Florida State University, USA. His research interests involve advanced electrical machines and drives for electric vehicles and renewable power generation.

Shuangxia Niu received the B.Sc. and M.Sc. degrees from Tianjin University, China, in 2002 and 2005, respectively, and the Ph.D. degree from the University of Hong Kong, Hong Kong, in 2009, all in electrical engineering. Currently she is an Associate Professor in the Department of Electrical Engineering at Hong Kong Polytechnic University, Hong Kong. She has authored or coauthored over 100 papers in leading journals. Her research interests are electrical machines and drives for electric vehicles, renewable energy conversion, and applied electromagnetics.

Xiaodong Zhang received the B.Eng. and M.Eng. degrees in Electrical Engineering from the Department of Automation, Tianjin University, China, in 2002 and 2005, respectively. He received the Ph.D. degree in electrical engineering from the Department of Electrical and Electronic Engineering, the University of Hong Kong, Hong Kong, in 2011. His research interests include design and control of electric machines for electric vehicles.

W.N. Fu received the B.Eng. degree from Hefei University of Technology, Hefei China, in 1982, the M.Eng. degree from Shanghai University of Technology, Shanghai, China, in 1989, and the Ph.D. degree from Hong Kong Polytechnic University, Hong Kong, in 1999, all in electrical engineering. He is currently a Professor at Hong Kong Polytechnic University. Before joining the university in 2007, he was one of the Key Developers at Ansoft Corporation, Pittsburgh, PA, USA. He has about seven years of working experience at Ansoft, focusing on the development of the commercial software Maxwell. His current research interests include electromagnetic field computation, applied electromagnetics, and novel electric machines.